JACS
JOURNAL OF THE AMERICAN CHEMICAL SOCIETY

Communication

Electrochemical Reduction of N2 into NH3 by Donor-Acceptor Couples of Ni and Au Nanoparticles with a 67.8% Faradaic Efficiency

Zhong-Hua Xue, Shi-Nan Zhang, Yun-Xiao Lin, Hui Su, Guang-Yao Zhai, Jing-Tan Han, Qiu-Ying Yu, Xin-Hao Li, Markus Antonietti, and Jie-Sheng Chen

J. Am. Chem. Soc., **Just Accepted Manuscript** • DOI: 10.1021/jacs.9b07963 • Publication Date (Web): 15 Sep 2019

Electrochemical Reduction of N_2 into NH_3 by Donor-Acceptor Couples of Ni and Au Nanoparticles with a 67.8% Faradaic Efficiency

Zhong-Hua Xue,[†] Shi-Nan Zhang,[†] Yun-Xiao Lin,[†] Hui Su,[†] Guang-Yao Zhai,[†] Jing-Tan Han[†], Qiu-Ying Yu[†], Xin-Hao Li[*†], Markus Antonietti,[‡] and Jie-Sheng Chen[†]

[†]School of Chemistry and Chemical Engineering, Shanghai Jiao Tong University, Shanghai 200240, P. R. China

[‡]Department of Colloid Chemistry, Max-Planck Institute of Colloids and Interfaces, Wissenschaftspark Golm, 14424 Potsdam, Germany

Supporting Information Placeholder

ABSTRACT: The traditional NH_3 production method (Haber-Bosch process) is currently complemented by electrochemical synthesis at ambient conditions, but the rather low selectivity (as indicated by the Faradaic efficiency) for the electrochemical reduction of molecular N_2 into NH_3 impedes the progress. Here, we present a powerful method to significantly boost the Faradaic efficiency of Au electrocatalysts to 67.8% for the nitrogen reduction reaction (NRR) by increasing their electron density through the construction of inorganic donor-acceptor couples of Ni and Au nanoparticles. The unique role of the electron-rich Au centres in facilitating the fixation and activation of N_2 was also been investigated via theoretical simulation methods and then confirmed by experimental results. The highly coupled Au and Ni nanoparticles supported on nitrogen-doped carbon are stable for reuse and long-term performance of the NRR, making the electrochemical process more sustainable for practical application.

Over the past century, ammonia (NH_3) synthesis was exclusively synthesized by the heterogeneously catalysed Haber-Bosch process, which annually consumes 1-2% of global energy production and simultaneously results in >1% of CO_2 emissions worldwide.[1–5] Concerning the availability of excess sustainable electricity, it is highly desirable for chemists to find alternative approaches to produce NH_3 via N_2 fixation, especially also locally and in a decentral fashion. However, the progress in N_2 fixation is challenged by the high activation barrier of the N_2 molecule, which is composed of a strong N-N triple bond, and the low selective absorption of the N_2 molecule, which has an extremely low polarizability, onto catalysts[6,7]. Recently, the electrochemical reduction of N_2 into NH_3 has shown great potential for activating molecular nitrogen under ambient conditions and at smaller scales.[8–12] The core focus of this ongoing research is the rational design of efficient and, most importantly, selective electrocatalysts to catalyse the proton-coupled 6-electron nitrogen reduction reaction (NRR) while retarding the competing 2-electron hydrogen evolution reaction (HER).[13–16]

To date, Au-based electrocatalysts, including nanostructured Au particles and metal-oxide-supported amorphous Au, are promising candidates for the electro-synthesis of NH_3 from N_2.[17–21] Much effort has been focused on nanostructure engineering to boost the reaction rate for the synthesis of ammonia, while a state-of-the-art Faradaic efficiency of 35% is still unsatisfactory for practical applications.[22–25] Again, developing efficient strategies to promote the selective absorption and activation of N_2 molecules on Au-based NRR electrocatalysts lies at the frontier of research on the ambient production of ammonia.

Here, we show that the rational arrangement of separated Au and Ni nanoparticles on/in nitrogen-doped carbon supports could generate an unusual case of inorganic donor-acceptor couples, significantly boosting the selectivity to ammonia in an aqueous electrolyte. The electron enrichment of Au nanoparticles was promoted by accepting electrons from the Ni nanoparticles due to the different work functions of the Au and Ni metals, resulting in facilitating the adsorption and dissociation of molecular N_2 over the electron-rich Au active sites and thus a remarkably high Faradaic efficiency for the NRR.

To rationally construct the donor-acceptor couples of Ni and Au nanoparticles, with a strong electronic connection between Au and Ni, for a highly selective NRR, we developed a straightforward Galvanic replacement method to deposit Au nanoparticles adjacent to Ni nanoparticles, as presented in Figure 1a. The atomic ratios of the Au-Ni couples in the Au/Ni samples (Figure 1b) were tuned by gradually increasing the amount of Au^{3+} with a fixed amount of Ni nanoparticles during the replacement process, while the chemical structure of the carbon support remained stable according to the XPS results (Figure S1). It should be noted that the Au content reaches a limiting value in the Au_{40}/Ni sample (Table S1) and no longer increases with the addition of more Au^{3+} because the Ni nanoparticles embedded inside the carbon matrix were not exposed to the solution-based replacement reaction. SEM and TEM observation (Figures S2–S3) further indicated similar foam-like structures for the carbon supports decorated with metal nanoparticles (mean size: ~ 17 nm) for the different Au_x/Ni samples. The XRD patterns directly identify the

presence of metallic Ni and Au nanoparticles (Figure 1c),[26–28] and indicate a clear trend of increasing Au content from the Ni to Au_{40}/Ni samples. Further, HAADF-TEM and the corresponding energy dispersive X-ray spectroscopy (EDX) elemental mapping images (Figure 1d–e and Figure S4) demonstrated the successful deposition of Au nanoparticles adjacent to the Ni nanoparticles on the nitrogen-doped carbon support.

Care was taken to exclude the possibility of the formation of Au-Ni bimetallic nanoparticles by analysing the EDX mapping results (Figures S4–S5). The high-resolution HAADF-STEM image (Figure 1f and Figure S6) of the Au nanoparticles with typical lattice fringes of 0.21 nm and 0.14 nm, which could be attributed to the (200) and (220) planes of metallic Au, respectively, further confirmed the formation of pristine Au nanostructures from the replacement of Ni nanoparticles.

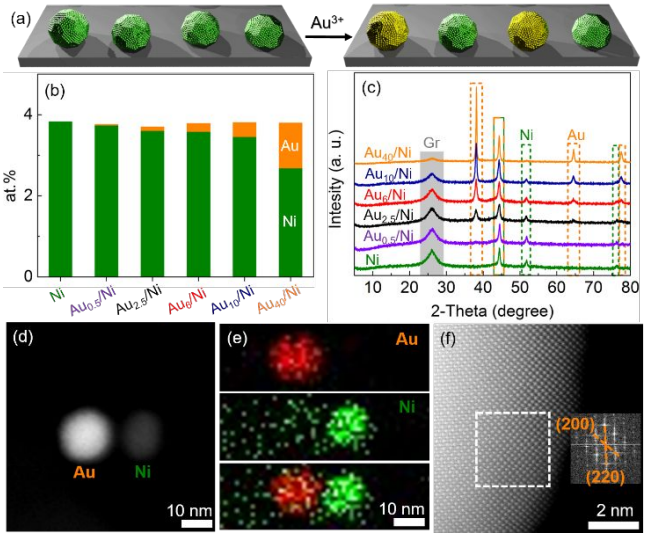

Figure 1. Preparation and structure. (a) Synthesis of donor-acceptor couples of Au and Ni nanoparticles. (b) Atomic content of Au and Ni as analysed by ICP and XPS and (c) XRD patterns of Ni and Au_x/Ni samples (x% represents the Au-to-Ni molar ratio). A typical (d) HAADF-TEM image, the corresponding (e) EDX mapping results and (f) HAADF-STEM image of Au_6/Ni. The inset in (f) shows the FFT pattern.

We initially evaluated the catalytic performance of the Au-Ni couple-based NRR electrocatalysts in an H-type cell (Figure S7). An obvious shift in the cyclic voltammetry curves of the Au/Ni samples, taking Au_6/Ni sample to a lower potential indicates a possible NRR in the electrolyte after saturation with N_2 gas to replace the Ar gas (Figure 2a). The yields of NH_3 were demonstrated by a Nessler reagent colorimetric method (Figure S8) and simultaneously confirmed by ion chromatography (Figure S9). Under increased work potential and current density (Figure 2b) outputs, the Au_6/Ni-based electrode, with an optimized catalyst loading of 2.0 mg cm^{-2} (Figure S10), offered the highest NH_3 yield of 7.4 μg h^{-1} mg^{-1}_{cat} and a Faradaic efficiency of 67.8% at −0.14 V (Figure 2c and Figure S11). Most importantly, the Au_6/Ni-based electrode also provided a stable current density for the NRR (Figure S12) and reproducible NH_3 yields and Faradaic efficiencies over six consecutive runs at −0.14 V vs. RHE (Figure 2d). Control experiments using an Ar-saturated electrolyte or a bare carbon cloth (Figures S13–S14) or blank reactions without current input (Figure S15) did not generate a detectable amount of NH_3. A ^{15}N isotopic labelling experiment further confirmed the formation of $^{15}NH_4^+$ (inset of Figure 2a and Figure S14) over the Au_6/Ni electrode under standard conditions.[10,29] The structure of the Au_6/Ni catalyst remained stable after prolonged NRR operation (Figure S16). All these results confirmed the efficient and stable NRR over the Au_6/Ni catalyst.

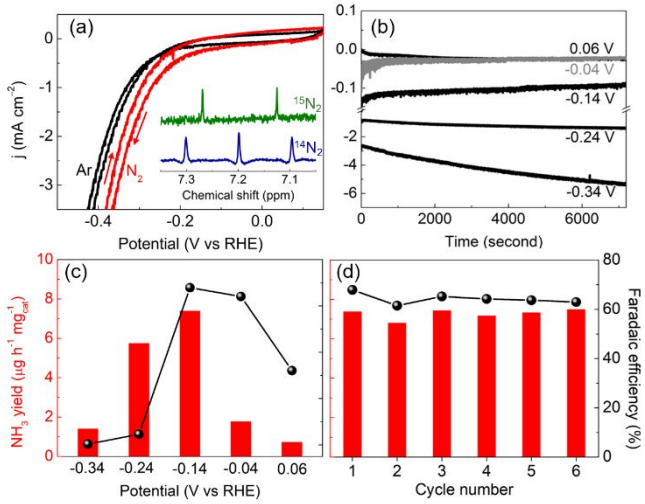

Figure 2. NRR activity over the Au_6/Ni catalyst. (a) CV curves in an N_2-saturated and Ar-saturated 0.05 M H_2SO_4 electrolyte. The inset of (a) shows the ^1H NMR spectra of the resultant electrolyte fed with $^{14}N_2$ and $^{15}N_2$. (b) Chronoamperometry results at different potentials. (c) NH_3 yield rate and Faradaic efficiency at the corresponding potentials and (d) during the recycling test.

The pristine Ni catalyst could deliver negligible NH_3 production (Figure 3a and Figure S17), but the incorporation of a small amount of Au triggers a significant NH_3 yield of 1.6 μg h^{-1} mg^{-1}_{cat} with a Faradaic efficiency of 14.2% over the $Au_{0.5}$/Ni catalysts, which has the lowest Au content of 0.28 wt%. The turnover frequency (TOF) of NRR over Au catalysts (Figure 3b) increased with decreasing Au contents, matching well with the trend of electron enrichment of the Au components, as indicated by the gradual shift of the Au 4f XPS peaks to lower binding energies (Figure 3d). It should be noted that the nitrogen-doped carbon-supported Ni nanoparticles have a relatively higher work function (6.86 eV) compared to that (6.75 eV) of the supported Au nanoparticles according to the ultraviolet photoelectron spectroscopy (UPS) results (Figures S18–S19), presumably due to the combination of the support effect (Figure S20) and size effect,[30–33] even though the theoretical work functions of bulk Au and Ni are all approximately 5.1 eV.[34] The Ni nanoparticles thus act as an electron donor here (Figure 3c), as further confirmed by an obvious shift of the Ni 2p XPS peaks to higher binding energies after the deposition of Au nanoparticles (Figure S21). All these results indicated the electron-enrichment-dependent NRR activity of the Au active centres. Indeed, the $Au_{0.5}$/Ni catalyst with the highest electron donor/acceptor ratio had the most pronounced electron enrichment and provided the highest TOF value (6.7 mol NH_3 mol^{-1} Au h^{-1}).

The electron-enrichment-dependent NRR activity of the Au catalysts was further confirmed by the positive correlation between the ammonia yields and the total electron densities (as indicated by the measured work functions) of the supported Au nanoparticles. After achieving a balance between the electron enrichment and the number of Au active centres for a fixed total content of the Au and Ni metals (Figure 3c), the Au component in the Au_6/Ni sample accepted the maximum total amount of electrons from the Ni and/or support and thus exhibited the lowest work function among all the Au_x/Ni samples (Figure 3f) and improved conductivity (Figure S22). Accordingly, the Au_6/Ni sample also performed as the best-in-class NRR catalyst in this paper and was used for the following characterizations and reactions.

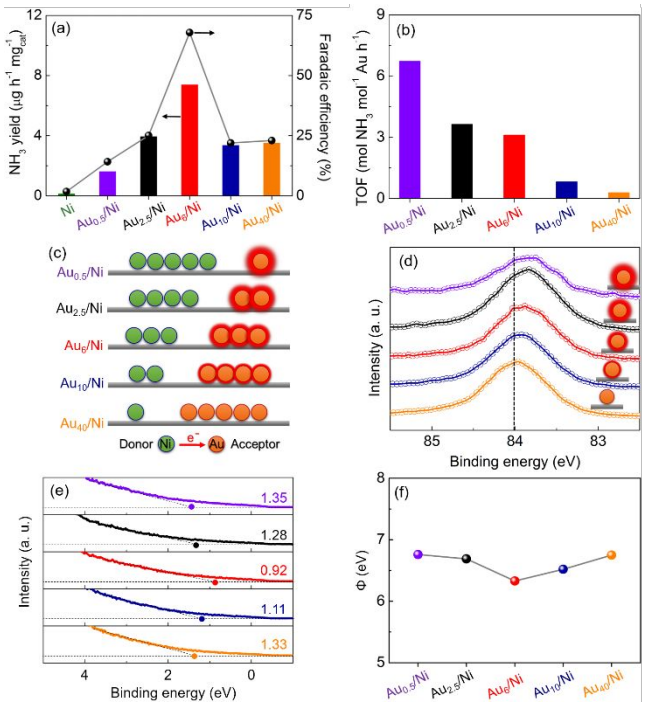

Figure 3. (a) NH_3 yield rate and Faradaic efficiency using the Ni and Au_x/Ni catalysts at -0.14 V vs. RHE. (b) TOF values of the NH_3 yield based on the Au content. (c) Electron transfer model for the donor-acceptor couples of Au and Ni nanoparticles. (d) Au 4f XPS spectra of the Au_x/Ni catalysts. Insets of (d) show the corresponding electron state models of Au. (e) UPS spectra in the onset (E_i) energy regions and (f) the measured work functions (Φ) via UPS analysis of the Au_x/Ni samples.

Computationally, we further investigated the possible roles of the electron-rich Au in accelerating the adsorption and activation of the N_2 molecules. Based on density functional theory (DFT) calculations and experimental results in pioneering works[17,35,36] and the calculated standard free energy diagram for the NRR in this work (Figure 4a), we propose an associative process on the Au, in which the dissociation of adsorbed N_2 (*N_2) into *NNH is the rate-limiting step, and the further splitting of *NNH_4 into NH_3 and *NH_2 by the addition of one proton proceeds automatically. Due to the similar configurations for each step of the NRR, the electron-rich Au catalyst (Au+e$^-$) significantly reduces the Gibbs free-energy (ΔG) of the rate-limiting N_2 dissociation step from 1.39 eV over a pristine Au catalyst to 1.13 eV, and the ΔG of the following three hydrogenation steps via *NNH_2 and *NNH_3 to *NNH_4. The polarization of the adsorbed N_2 molecules induced by the electron-rich Au surface, which benefits the further addition of a hydrogen atom to the electron-deficient N, was well presented by the obvious differences in the electron densities (Hirshfeld charge) of each N atom after changing the catalytic surface from the Au to the electron-rich Au models (Figure 4b and Figure S23). Such a strong polarizing effect also enhanced the pre-adsorption of N_2 molecules onto the electron-rich Au surface, as theoretically predicted by the much higher adsorption energy, and then validated experimentally by the stronger N_2 adsorption peak in the N_2 temperature-programmed desorption (TPD) isotherm of the Au_6/Ni sample (Figure 4d and Figure S24). It was also found that the desorption energy of the NH_3 molecule decreased on the electron-rich Au surface (Figure 4c), indicating a rapid release of the active site for new reactions.

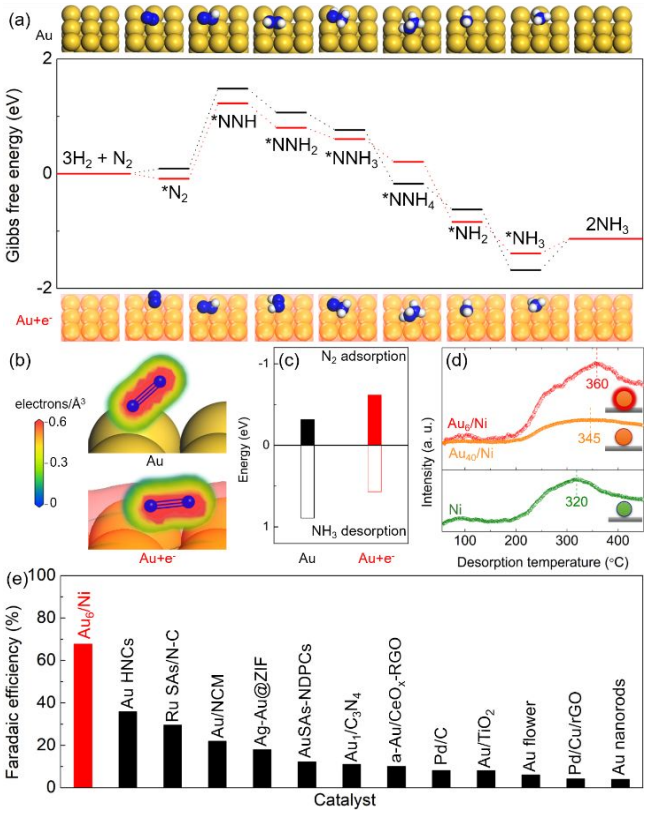

Figure 4. (a) Gibbs free energy diagram of the NRR for Au and electron-rich Au. The insets show the corresponding optimized absorption structures. (b) The calculated electron density maps for N_2 adsorbed onto the surface of Au and electron-rich Au (Au+e$^-$). (c) The calculated adsorption energies of N_2 and desorption energies of NH_3 adsorbed onto Au and Au+e$^-$. (d) The N_2-TPD results of the Ni, Au_6/Ni and Au_{40}/Ni catalysts normalized by the Au content. The insets show the corresponding structural models. (e) Faradaic efficiencies for the NRR over various noble-metal-based electrocatalysts.

Taken together, a rational construction of electron-rich Au nanoparticles with an optimal ratio of the Ni-Au donor-acceptor pairs could promote the activity of the whole NRR process by enhancing the pre-adsorption and activation of N_2 and facilitating the desorption of ammonia. As a result, the Au_6/Ni catalyst provided a high Faradaic efficiency of greater than 67.8%, far outperforming the values of all reported Au-,[17–25,37] Ru-,[38] or Pd-based[39,40] electrocatalysts (Figure 4e and Table S2).

In summary, inorganic donor-acceptor couples of Ni and Au nanoparticles have been designed to improve the highly selective nitrogen reduction reaction. Both the experimental and theoretical results demonstrated the key role of the as-formed electron-rich Au nanoparticles, which accept electrons from the Ni nanoparticles, in facilitating the adsorption and activation of N_2 molecules and producing a high Faradaic efficiency of 67.8% at -0.14 V vs. RHE in an acidic electrolyte. This work offers a guideline for the fabrication of electrocatalysts using metal-metal electron transfer to achieve high selectivity for electrochemical nitrogen fixation in combination with novel reactors for practical uses and provides a direct and intriguing method to develop highly efficient catalysts for the challenging activation of small molecules.

ASSOCIATED CONTENT

Supporting Information

Experimental details, more characterization results, and detailed discussions. This material is available free of charge via the Internet at http://pubs.acs.org

AUTHOR INFORMATION

Corresponding Author

xinhaoli@sjtu.edu.cn (XHL)

Notes

The authors declare no competing financial interests.

ACKNOWLEDGMENT

This work was supported by the National Natural Science Foundation of China (21722103, 21720102002, and 21673140), the Shanghai Basic Research Program (16JC1401600), and the SJTU-MPI partner group.

REFERENCES

(1) Gruber, N.; Galloway, J. N. An Earth-system perspective of the global nitrogen cycle. *Nature* **2008**, *451*, 293–296.
(2) Service, R. F. New recipe produces ammonia from air, water, and sunlight. *Science* **2014**, *345*, 610.
(3) Erisman, J. W.; Sutton, M. A.; Galloway, J.; Klimont, Z.; Winiwarter, W. How a century of ammonia synthesis changed the world. *Nat. Geosci*. **2008**, *1*, 636–639.
(4) Chen, J. G.; Crooks, R. M.; Seefeldt, L. C.; Bren, K. L.; Bullock, R. M.; Darensbourg, M. Y.; Holland, P. L.; Hoffman, B.; Janik, M. J.; Jones, A. K.; Kanatzidis, M. G.; King, P.; Lancaster, K. M.; Lymar, S. V.; Pfromm, P.; Schneider, W. F.; Schrock, R. R. Beyond fossil fuel–driven nitrogen transformations. *Science* **2018**, *360*, eaar6611.
(5) Martín, A. J.; Shinagawa, T.; Pérez-Ramírez, J. Electrocatalytic reduction of nitrogen: from Haber-Bosch to ammonia artificial leaf. *Chem* **2019**, *5*, 263–283.
(6). Singh, A. R.; Rohr, B. A.; Schwalbe, J. A.; Cargnello, M.; Chan, K.; Jaramillo, T. F.; Chorkendorff, I.; Nørskov, J. K. Electrochemical ammonia synthesis-the selectivity challenge. *ACS Catal*. **2017**, *7*, 706–709.
(7) van der Ham, C. J. M.; Koper, M. T. M.; Hetterscheid, D. G. H. Challenges in reduction of dinitrogen by proton and electron transfer. *Chem. Soc. Rev*. **2014**, *43*, 5183–5191.
(8) Guo, C.; Ran, J.; Vasileff, A.; Qiao, S.-Z. Rational design of electrocatalysts and photo(electro)catalysts for nitrogen reduction to ammonia (NH_3) under ambient conditions. *Energy Environ. Sci*. **2018**, *11*, 45–56.
(9) Cui, X.; Tang, C.; Zhang, Q. A review of electrocatalytic reduction of dinitrogen to ammonia under ambient conditions. *Adv. Energy Mater*. **2018**, *8*, 1800369.
(10) Suryanto, B. H. R.; Du, H.-L.; Wang, D.; Chen, J.; Simonov, A. N.; MacFarlane, D. R. Challenges and prospects in the catalysis of electroreduction of nitrogen to ammonia. *Nat. Catal*. **2019**, *2*, 290–296.
(11) Song, Y.; Johnson, D.; Peng, R.; Hensley, D. K.; Bonnesen, P. V.; Liang, L.; Huang, J.; Yang, F.; Zhang, F.; Qiao, R.; Baddorf, A. P.; Tschaplinski, T. J.; Engle, N. L.; Hatzell, M. C.; Wu, Z.; Cullen, D. A.; Meyer III, H. M.; Sumpter, B. G.; Rondinone, A. J. A physical catalyst for the electrolysis of nitrogen to ammonia. *Sci. Adv*. **2018**, *4*, e1700336.
(12) Qiu, W.; Xie, X.-Y.; Qiu, J.; Fang, W.-H.; Liang, R.; Ren, X.; Ji, X.; Cui, G.; Asiri, A. M.; Cui, G.; Tang, B.; Sun, X. High-performance artificial nitrogen fixation at ambient conditions using a metal-free electrocatalyst. *Nat. Commun*. **2018**, *9*, 3485.
(13) Foster, S. L.; Bakovic, S. I. P.; Duda, R. D.; Maheshwari, S.; Milton, R. D.; Minteer, S. D.; Janik, M. J.; Renner, J. N.; Greenlee, L. F. Catalysts for nitrogen reduction to ammonia. *Nat. Catal*. **2018**, *1*, 490–500.
(14) Wang, M.; Liu, S.; Qian, T.; Liu, J.; Zhou, J.; Ji, H.; Xiong, J.; Zhong, J.; Yan, C. Over 56.55% Faradaic efficiency of ambient ammonia synthesis enabled by positively shifting the reaction potential. *Nat. Commun*. **2019**, *10*, 341.
(15) Hao, Y.-C.; Guo, Y.; Chen, L.-W.; Shu, M.; Wang, X.-Y.; Bu, T.-A.; Gao, W.-Y.; Zhang, N.; Su, X.; Feng, X.; Zhou, J.-W.; Wang, B.; Hu, C.-W.; Yin, A.-X.; Si, R.; Zhang, Y.-W.; Yan, C.-H. Promoting nitrogen electroreduction to ammonia with bismuth nanocrystals and potassium cations in water. *Nat. Catal*. **2019**, *2*, 448–456.
(16) Xue, Z.-H.; Su, H.; Yu, Q.-Y.; Zhang, B.; Wang, H.-H.; Li, X.-H.; Chen, J.-S. Janus Co/CoP nanoparticles as efficient Mott–Schottky electrocatalysts for overall water splitting in wide pH range. *Adv. Energy Mater*. **2017**, *7*, 1602355.
(17) Bao, D.; Zhang, Q.; Meng, F.-L.; Zhong, H.-X.; Shi, M.-M.; Zhang, Y.; Yan, J.-M.; Jiang, Q.; Zhang, X.-B. Electrochemical reduction of N_2 under ambient conditions for artificial N_2 fixation and renewable energy storage using N_2/NH_3 cycle. *Adv. Mater*. **2017**, *29*, 1604799.
(18) Nazemi, M.; Panikkanvalappil, S. R.; El-Sayed, M. A. Enhancing the rate of electrochemical nitrogen reduction reaction for ammonia synthesis under ambient conditions using hollow gold nanocages. *Nano Energy*, **2018**, *49*, 316–323.
(19) Wang, Z.; Li, Y.; Yu, H.; Xu, Y.; Xue, H.; Li, X.; Wang, H.; Wang, L. Ambient electrochemical synthesis of ammonia

from nitrogen and water catalyzed by flower-like gold microstructures. *ChemSusChem*, **2018**, *11*, 3480–3485.
(20) Li, S.-J.; Bao, D.; Shi, M.-M.; Wulan, B.-R.; Yan, J.-M.; Jiang, Q. Amorphizing of Au nanoparticles by CeO_x–RGO hybrid support towards highly efficient electrocatalyst for N_2 reduction under ambient conditions. *Adv. Mater.* **2017**, *29*, 1700001.
(21) Shi, M.-M.; Bao, D.; Wulan, B.-R.; Li, Y.-H.; Zhang, Y.-F.; Yan, J.-M.; Jiang, Q. Au sub-nanoclusters on TiO_2 toward highly efficient and selective electrocatalyst for N_2 conversion to NH_3 at ambient conditions. *Adv. Mater.* **2017**, *29*, 1606550.
(22) Wang, H.; Wang, L.; Wang, Q.; Ye, S.; Sun, W.; Shao, Y.; Jiang, Z.; Qiao, Q.; Zhu, Y.; Song, P.; Li, D.; He, L.; Zhang, X.; Yuan, J.; Wu, T.; Ozin, G. A. Ambient electrosynthesis of ammonia: electrode porosity and composition engineering. *Angew. Chem. Int. Ed.* **2018**, *57*, 12360–12364.
(23) Qin, Q.; Heil, T.; Antonietti, M.; Oschatz, M. Single-site gold catalysts on hierarchical N-doped porous noble carbon for enhanced electrochemical reduction of nitrogen. *Small Methods* **2018**, *2*, 1800202.
(24) Wang, X.; Wang, W.; Qiao, M.; Wu, G.; Chen, W.; Yuan, T.; Xu, Q.; Chen, M.; Zhang, Y.; Wang, X.; Wang, J.; Ge, J.; Hong, X.; Li, Y.; Wu, Y.; Li, Y. Atomically dispersed Au$_1$ catalyst towards efficient electrochemical synthesis of ammonia. *Sci. Bull.* **2018**, *63*, 1246–1253.
(25) Nazemi, M.; El-Sayed, M. A. Electrochemical synthesis of ammonia from N_2 and H_2O under ambient conditions using pore-size-controlled hollow gold nanocatalysts with tunable plasmonic properties. *J. Phys. Chem. Lett.* **2018**, *9*, 5160–5166.
(26) Xue, Z.-H.; Han, J.-T.; Feng, W.-J.; Yu, Q.-Y.; Li, X.-H.; Antonietti, M.; Chen, J.-S. Tuning the adsorption energy of methanol molecules along Ni-N-doped carbon phase boundaries by the Mott–Schottky effect for gas-phase methanol dehydrogenation. *Angew. Chem. Int. Ed.* **2018**, *57*, 2697–2701.
(27) Kim, D.; Xie, C.; Becknell, N.; Yu, Y.; Karamad, M.; Chan, K.; Crumlin, E. J.; Nørskov, J. K.; Yang, P. Electrochemical activation of CO_2 through atomic ordering transformations of AuCu nanoparticles. *J. Am. Chem. Soc.* **2017**, *139*, 8329–8336.
(28) Zhang, P.; Wang, L.; Yang, S.; Schott, J. A.; Liu, X.; Mahurin, S. M.; Huang, C.; Zhang, Y.; Fulvio, P. F.; Chisholm, M. F.; Dai, S. Solid-state synthesis of ordered mesoporous carbon catalysts via a mechanochemical assembly through coordination cross-linking. *Nat. Commun.* **2017**, *8*, 15020.
(29) Andersen, S. Z.; Čolić, V.; Yang, S.; Schwalbe, J. A.; Nielander, A. C.; Mcenaney, J. M.; Enemark-Rasmussen, K.; Baker, J. G.; Singh, A. R.; Rohr, B. A.; Statt, M. J.; Blair, S. J.; Mezzavilla, S.; Kibsgaard, J.; Vesborg, P. C. K.; Cargnello, M.; Bent, S. F.; Jaramillo, T. F.; Stephens, I. E. L.; Nørskov, J. K.; Chorkendorff, I. A rigorous electrochemical ammonia synthesis protocol with quantitative isotope measurements. *Nature* **2019**, *570*, 504–508.
(30) Su, H.; Zhang, K.-X.; Zhang, B.; Wang, H.-H.; Yu, Q.-Y.; Li, X.-H.; Antonietti, M.; Chen, J.-S. Activating cobalt nanoparticles via the Mott–Schottky effect in nitrogen-rich carbon shells for base-free aerobic oxidation of alcohols to esters. *J. Am. Chem. Soc.* **2017**, *139*, 811–818.
(31) Li, X.-H.; Chen, J.-S.; Wang, X.; Sun, J.; Antonietti, M. Metal-free activation of dioxygen by graphene/g-C_3N_4 nanocomposites: Functional dyads for selective oxidation of saturated hydrocarbons. *J. Am. Chem. Soc.* **2011**, *133*, 8074–8077.
(32) Liu, Y.-X.; Wang, H.-H.; Zhao, T.-J.; Zhang, B.; Su, H.; Xue, Z.-H.; Li, X.-H.; Chen, J.-S. Schottky barrier induced coupled interface of electron-rich N-doped carbon and electron-deficient Cu: In-built Lewis acid–base pairs for highly efficient CO_2 fixation. *J. Am. Chem. Soc.* **2019**, *141*, 38–41.
(33) Meng, J.; Niu, C.; Xu, L.; Li, J.; Liu, X.; Wang, X.; Wu, Y.; Xu, X.; Chen, W.; Li, Q.; Zhu, Z.; Zhao, D.; Mai, L. General oriented formation of carbon nanotubes from metal–organic frameworks. *J. Am. Chem. Soc.* **2017**, *139*, 8212–8221.
(34) Li, X.-H.; Antonietti, M. Metal nanoparticles at mesoporous N-doped carbons and carbon nitrides: functional Mott–Schottky heterojunctions for catalysis. *Chem. Soc. Rev.* **2013**, *42*, 6593–6604.
(35) Skúlason, E.; Bligaard, T.; Gudmundsdóttir, S.; Studt, F.; Rossmeisl, J.; Abild-Pedersen, F.; Vegge, T.; Jónssonac, H.; Nørskov, J. K. A theoretical evaluation of possible transition metal electro-catalysts for N_2 reduction. *Phys. Chem. Chem. Phys.* **2012**, *14*, 1235–1245.
(36) Yao, Y.; Zhu, S.; Wang, H.; Li, H.; Shao, M. A spectroscopic study on the nitrogen electrochemical reduction reaction on gold and platinum surfaces. *J. Am. Chem. Soc.* **2018**, *140*, 1496–1501.
(37) Lee, H. K.; Koh, C. S. L.; Lee, Y. H.; Liu, C.; Phang, I. Y.; Han, X.; Tsung, C.-K.; Ling, X. Y. Favoring the unfavored: Selective electrochemical nitrogen fixation using a reticular chemistry approach. *Sci. Adv.* **2018**, *4*, eaar3208.
(38) Geng, Z.; Liu, Y.; Kong, X.; Li, P.; Li, K.; Liu, Z.; Du, J.; Shu, M.; Si, R.; Zeng, J. Achieving a record-high yield rate of 120.9 μg_{NH_3} $mg^{-1}_{cat.}$ h^{-1} for N_2 electrochemical reduction over Ru single-atom catalysts. *Adv. Mater.* **2018**, *30*, 1803498.
(39) Wang, J.; Yu, L.; Hu, L.; Chen, G.; Xin, H.; Feng, X. Ambient ammonia synthesis via palladium-catalyzed electrohydrogenation of dinitrogen at low overpotential. *Nat. Commun.* **2018**, *9*, 1795.
(40) Shi, M.-M.; Bao, D.; Li, S.-J.; Wulan, B.-R.; Yan, J.-M.; Jiang, Q. Anchoring PdCu amorphous nanocluster on graphene for electrochemical reduction of N_2 to NH_3 under ambient conditions in aqueous solution. *Adv. Energy Mater.* **2018**, *8*, 1800124.

SYNOPSIS TOC